

Simulation of DNA Damage after Proton Irradiation

Werner Friedland,¹ Peter Jacob, Philipp Bernhardt, Herwig G. Paretzke and Michael Dingfelder

GSF-National Research Center for Environment and Health, Institute of Radiation Protection, 85764 Neuherberg, Germany

Friedland, W., Jacob, P., Bernhardt, P., Paretzke, H. G. and Dingfelder, M. Simulation of DNA Damage after Proton Irradiation. *Radiat. Res.* 159, 401–410 (2003).

The biophysical radiation track simulation model PARTRAC was improved by implementing new interaction cross sections for protons in water. Computer-simulated tracks of energy deposition events from protons and their secondary electrons were superimposed on a higher-order DNA target model describing the spatial coordinates of the whole genome inside a human cell. Induction of DNA double-strand breaks was simulated for proton irradiation with LET values between 1.6 and 70 keV/ μm and various reference radiation qualities. The yield of DSBs after proton irradiation was found to rise continuously with increasing LET up to about 20 DSBs per Gbp and Gy, corresponding to an RBE up to 2.2. About half of this increase resulted from a higher yield of DSB clusters associated with small fragments below 10 kbp. Exclusion of experimentally unresolved multiple DSBs reduced the maximum DSB yield by 30% and shifted it to an LET of about 40 keV/ μm . Simulated fragment size distributions deviated significantly from random breakage distributions over the whole size range after irradiation with protons with an LET above 10 keV/ μm . Determination of DSB yields using equations derived for random breakage resulted in an underestimation by up to 20%. The inclusion of background fragments had only a minor influence on the distribution of the DNA fragments induced by radiation. Despite limited numerical agreement, the simulations reproduced the trends in proton-induced DNA DSBs and fragment induction found in recent experiments.

© 2003 by Radiation Research Society

INTRODUCTION

The induction of DNA double strand breaks (DSBs) after irradiation is thought to be of fundamental importance for producing radiation-induced death and injury to cells (1). The reproduction of measured radiation-induced yields of DSBs can be taken as a benchmark for Monte Carlo models for calculation of radiation damage to DNA and as a prerequisite for confidence in the results of simulations of other radiation effects where direct measurements are not possible.

Previous measurements of DSB yields showed only slight variation with radiation quality (2, 3). After proton irradiation, RBE values for DSB induction, relative to 200 to 250 kVp X rays, were found to be within the range between 0.8 and 1.1 using the sedimentation technique as well as filter elution (4–6). Recent measurements using constant-field gel electrophoresis (CFGE) or pulsed-field gel electrophoresis (PFGE) have resulted in higher yields and RBE values between 1.24 and 2.03 and in an evident increase with increasing LET (7–9).

A comparison between measured and calculated results must also take into account a possible bias because of the experimental techniques used and the methods of data analysis. Different methods for the quantification of X-ray-induced DNA DSBs after PFGE under the assumption of randomly induced breaks were investigated and gave essentially the same results (10). Recently, however, a study to assess the applicability of methods to quantify of X-ray and α -particle-induced DSBs based on the random breakage paradigm resulted in different RBE values, depending on how the methods were employed (11). The question remained open regarding how well the production of correlated breaks on the chromatin loops structures from single particle traversals could explain the deviations from the predictions of the random breakage assumption. Considerably different DSB yields were reported after proton and ^4He -ion irradiation when different methods of analysis were used (12).

Another possible source of an incorrect estimation of breakage frequencies was claimed to result from background DNA fragment distributions obtained from treatment of unirradiated cells (13). In the conventional analysis of PFGE experiments, a background distribution is simply subtracted from the distribution measured for irradiated cells for each molecular weight region; however, this approach may be an oversimplification (14).

In the present work, DSB yields and DNA fragment distributions after proton irradiation were simulated over a wide range of LET values in an extension of a recent pilot study (15). The investigation assesses in particular (1) the contribution of correlated breaks to the total DNA DSB induction, (2) a possible bias introduced by the use of algorithms based on the random breakage assumption, and (3) the influence of a background distribution on the radi-

¹ Address for correspondence: GSF-National Research Center for Environment and Health, Institute of Radiation Protection, Ingolstädter Landstr. 1, D-85764 Neuherberg, Germany; Email: friedland@gsf.de.

ation-induced DNA fragment distribution. These are done, respectively, by (1) subtracting correlated DSB associated with DNA fragment sizes less than the experimental resolution limit from the simulated total number of DSBs, (2) applying algorithms used for the derivation of DSB yields from measured DNA fractions to simulated DNA fragment size distributions, and (3) simulating radiation-induced DNA fragmentation on the basis of a genome bearing a background distribution of DNA fragments. The simulations were performed with the Monte Carlo track structure code PARTRAC (16, 17) after implementing new cross sections for protons.

MATERIALS AND METHODS

The Monte Carlo code PARTRAC and its main simulation modules as well as DNA target structure models, electron and photon track structure simulation, and DNA strand break induction from direct and indirect effects were described in detail elsewhere (16, 17). Therefore, this section focuses on further development of the model and specification of parameter sets used.

Proton Track Structure Simulation

A new module for the simulation of proton tracks was implemented in the Monte Carlo track structure simulation code PARTRAC. The track structure simulation was performed using the classical trajectory picture that follows the primary proton as well as all secondary electrons produced from starting or ejection energy down to total stopping (a few eV in case of electrons, 1 keV in case of protons or neutral hydrogen), by processing elastic and inelastic, including charge-changing scattering events. When a proton slows down, it can produce direct ionization or excitation events, but it can also capture an electron from a target molecule, converting itself into a neutral hydrogen atom. The neutral hydrogen atom itself can ionize or excite, or lose the electron again, converting itself back into a proton.

We recently derived new cross sections for inelastic interactions of energetic protons and neutral hydrogen atoms in liquid water (18). Liquid water was used as a model substance for the biological material under consideration. The data set covered a proton energy range from 1 keV up to 10 GeV and considered the following interaction processes: ionization, excitation and electron capture from target molecules for protons, and ionization and electron stripping for neutral hydrogen atoms. Neglected in this model were excitation by neutral hydrogen atoms as well as elastic scattering of the proton; both processes are only of minor effect in this context.

Ionization and excitation cross sections were determined within the (non-relativistic) plane-wave first Born approximation (PWBA). In this approximation, the double differential (in energy and momentum transfer) cross section was related to the dielectric response function, which had been determined in a semi-empirical model for liquid water before (19). The Bethe approximation was used for the extension to relativistic energies, while semi-empirical approaches were applied for energies below 500 keV where the PWBA is no longer valid. Charge transfer and stripping cross sections were represented by simple analytical functions following general trends of experimental data. Parameters were also determined and adjusted by comparing calculated stopping powers, to which all processes and charge states contribute, with the ICRU recommendations (20) for water and other experimental data as described in refs. (18) and (21).

Secondary electron emission spectra (angular distributions) were modeled within the framework of the non-relativistic Bethe theory, i.e. as a superposition of the binary encounter peak (hard collisions) and the dipole interaction (close or glancing collisions). Identical distributions were

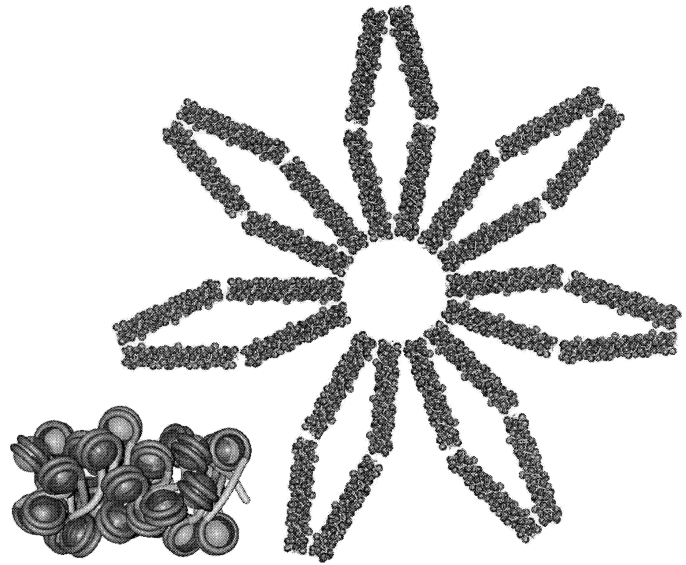


FIG. 1. Basic chromatin fiber element including 30 nucleosomes and an ideal arrangement of chromatin fiber rods in rhombic loops forming a rosette-like structure of 0.5 Mbp genomic length.

assumed for interactions of protons and neutral hydrogen atoms. More details and angular distributions can be found elsewhere (21).

DNA Target Model

The DNA target model was designed to represent the genome of a human fibroblast in its interphase. The total genomic length was assumed to be 6 Gbp. The basic element of the model is shown in Fig. 1. It consists of a repetitive piece of a chromatin fiber 50 nm long formed by an arrangement of 30 nucleosomes with a total of 6008 bp in atomic resolution. The nucleosomes were organized in a stochastic crossed-linker structure with an average angle of 150° between succeeding nucleosomes and a mean radial distance of 11 nm between the center of the histone and the fiber axis. The positions of the histones and the orientations of their axes within the basic element deviated stochastically from a regular symmetrical assembly within the chromatin fiber. Interpenetration of the DNA helices with each other and with the histones was inhibited. Three of the basic fiber elements were stacked together, making a 150-nm- or 18-kbp-long chromatin fiber rod that was the essential component of the chromatin organization within the nucleus.

The cylindrical shape of the cell nucleus was divided in this model into 46 territories, each with a volume proportional to the length of the corresponding chromosome, plus an additional non-contiguous volume, comprising 5% of the nuclear volume, that was not occupied by chromosomes. The territories were specified by thousands of contiguous cubic grid elements with a side length of 150 nm. Within these territories the chromosomes were established by a chain of chromatin fiber rods. Succeeding fiber rods started near the ends of the former ones, with a sequence of deflection angles which produced ideally narrow rhombic fiber loops 72 kbp in length, with a rosette-like structure of 0.5 Mbp found from seven of these rhombuses (Fig. 1). During the simulation calculation, these perfect structures were veiled due to the accumulation of the small stochastic variations of starting points and angles that were necessary to generate non-overlapping fiber structures. Larger deflection angles and increased gaps between the rods were applied whenever the scheme continued to result in overlapping configurations within the chromosomal territory even after a large number of trials. In the present realization, the geometric distances for genomic intervals below 0.1 Mbp were smaller than in earlier simulation calculations including the pilot study (15) where a slightly less condensed chromatin fiber rod with 60

nucleosomes per 108 nm and more spacious loops of 11 fiber rods had been used.

Calculation of the Induction of Single- and Double-Strand Breaks

For an optimum determination of absolute yields of SSBs and DSBs, model parameters were adjusted so as to produce approximately the following results for ^{60}Co γ rays from the literature: a DSB yield of about $8 \text{ Gy}^{-1} \text{ Gbp}^{-1}$ (22), a ratio of SSBs to DSBs of about 20:1 (23), and a ratio of breaks from direct and indirect effects of about 35:65 (24); this relationship differs from earlier PARTRAC simulations (17).

The simulated yield of DNA strand breaks due to direct and quasi-direct (non-scavengable) effects was determined from a superposition of the track structure pattern of inelastic events with the DNA target model. The effective target volume was given by union of the atoms in the sugar-phosphate backbone of the DNA applying a van der Waals radius multiplier of 2. The increased radii were intended to account for an inclusion of a water shell with 10 molecules per nucleotide in the target volume. The fraction of events in that volume that produced a DNA strand break was no longer determined by a selected threshold energy but was assumed to increase linearly from 0 at 5 eV to 1 for a deposited energy of 37.5 eV that had resulted from parameter adjustment. The lower limit of 5 eV was adopted from recent experiments showing that DNA strand breaks are induced by photons and electrons with energies well below 10 eV (25, 26).

The simulation of DNA strand breaks from indirect effects started with energy deposition events and thermalized electrons occurring inside a cylinder with a 25-nm diameter positioned around the chromatin fiber axis within bulk water found in all the volume occupied by neither atoms of the DNA (applying a van der Waals multiplier of 2) nor histones. The histones were modeled by spheres of 4.5 nm radius in which up to one-half of the DNA double helix was embedded, similar to the approach in ref. (27). Ionized and excited water molecules were assumed to dissociate, producing the reactive species e^-_{aq} , H_3O^+ , OH^\bullet , H^\bullet and H_2 . The dissociation scheme and relaxation probabilities as well as the parameters for diffusion and interaction of these reactive species were taken from ref. (28). For the interaction of OH radicals and hydrated electrons with constituents of the DNA, reaction radii derived from rate constants of Buxton *et al.* (29) were used. Additionally, OH radicals were assumed to be scavenged after an encounter with histones using a radius of 4.5 nm as the interaction distance. Other chemically reactive species were assumed not to interact either with DNA or with histones, but were forced not to diffuse into the volume occupied by these molecules. "Jump-through" corrections (30) were considered for reactions among species as well as reactions with DNA constituents.

Strand breaks from indirect (scavengable) effects were assumed to occur in 13% of the interactions of OH radicals with DNA (31). Since the contribution of interactions with the sugar moiety provided about 18.5% of the total OH $^\bullet$ -DNA interactions in the actual simulation, a breakage probability factor of 0.7 was applied to OH radical interactions with deoxyribose. In earlier calculations the process of OH radical scavenging by low-molecular-weight components occurring in the cellular water had been taken into account by a survival probability for each time step. In the present work a time-limited simulation was applied; differences between these approaches and an encounter-controlled simulation were found to be tolerable in computer simulations (32). From parameter adjustment a time limit of 10 ns was chosen which discarded only a small fraction of breaks from indirect effects.

The induction of a DSB was assumed whenever two single-strand breaks were found within 10 bp on opposite DNA strands. Experimental results for low-energy electron (25) and photon irradiations (26) of plasmid DNA as well as other studies (33) indicate that DSBs may also be produced with some probability in succession of one single SSB without a further event at the opposite strand; the corresponding percentage of transfer processes ranges from 0.8% to 6%. In the present work, a conversion into a DSB was assumed for 1% of all breaks produced by both

direct and indirect effects irrespective of further characteristics of the break.

Comparisons with Experimental Data

In the comparison of simulated results with experimental data, the constraints of the experimental procedures regarding the inclusion of short DNA fragments were taken into account. Frankenberg *et al.* (7) found that DNA molecules of up to 10 kbp were lost completely; thus pairs or clusters of DSB breaks within that genomic distance are not resolved in the experiments. Therefore, the numbers of DNA fragments smaller than this limit of 10 kbp were subtracted from the total number of induced DSBs; the result was denoted "distant DSB".

In the analysis of DNA DSB measurements using CFGE or PFGE, DSB yields are often determined from the overall fraction of activity released out of the well (FAR). The yields are calculated from the data on FAR using formulas derived for random breakage distributions by matching calculated and measured FAR values for a certain gel exclusion size, which has to be determined separately. Modifications may be included to take into account the maximum fraction of cellular DNA that can effectively enter the gel and the contribution of background fragments. DSB yields per unit dose are typically determined from a linear regression of the DSB yields as a function of the doses administered.

In this work the same technique was applied to simulated distributions of DNA fragments using the equation derived for random distributions (34),

$$F_{<K}(D) = 1 - \left[1 + \frac{K\mu(D)}{S} \left(1 - \frac{K}{S} \right) \right] \exp \left(-\frac{K\mu(D)}{S} \right), \quad (1)$$

where $F_{<K}$ is the DNA fraction found in fragments smaller than the gel exclusion size K , S is the mean size of the chromosomes, and $\mu(D)$ is the average number of DSBs per average chromosome size S after irradiation with dose D . The DSB yield, given in breaks per Gy and Gbp, was determined from $Y_D = \mu(D)/(S \cdot D)$ and from linear regression of these values of $\mu(D)$ for applied doses of 10, 33, 50 and 100 Gy. The dependence of these DSB yields on gel exclusion size and applied dose provides information about possible bias introduced by this analysis method due to deviations from random breakage.

In addition to the integral result, DSB yields per dose were also determined as a function of the DNA fragment size. This conversion from DNA fragment distributions was performed for the simulated data using the equation derived for randomly broken fragments (35),

$$F(k, D)dk = \frac{\mu(D)}{S} \left(2 + \mu(D) - \frac{k\mu(D)}{S} \right) \exp \left(-\frac{k\mu(D)}{S} \right) dk, \quad (2)$$

where $F(k, D)dk$ is the fraction of DNA found in the fragment size interval $[k, k+dk]$ and the other symbols as above. The DSB yields $Y = \mu(D)/(S \cdot D)$ were determined recursively from the DNA fractions in 10 logarithmic equidistant intervals per decade. It must be noted that this function (2) has a maximum value, and the recursion of DSB yields therefore has two solutions for a fraction below its maximum but no solution for a fraction above the maximum. Experimental data for small DNA fragments are typically located on the increasing branch of the function. Around the maximum of the distribution the determination of a DSB yield has a large uncertainty. A discontinuity due to a transition to the decreasing branch may occur near the maximum of a simulated fraction that is smaller than the maximum of the random breakage distribution.

After treatment of unirradiated control cells, the number N of DNA fragments with sizes in the interval $[k, k+dk]$ was found to follow approximately a power-law function (13),

$$N(k)dk = A \cdot k^B dk, \quad (3)$$

with the parameters A and B . Distributions of DNA fragments F_{bg} corresponding to a power-law function with exponent B in the size interval $[k_{min}, k_{max}]$ were generated from random numbers R in the interval $[0, 1]$ according to

TABLE 1
Calculated Yields of SSBs, Total DSBs, Distant DSBs, and DSBs from FAR Analysis

Radiation quality	LET ^a L _{∞,D} (keV/μm)	SSB yield (Gbp ⁻¹ Gy ⁻¹)	Yield of total DSBs (Gbp ⁻¹ Gy ⁻¹)	Yield of “distant” DSBs ^b (Gbp ⁻¹ Gy ⁻¹)	DSB yield from FAR analysis ^c (Gbp ⁻¹ Gy ⁻¹)
50 MeV protons	1.6	195	8.6	8.2	8.0
20 MeV protons	2.7	191	9.1	8.7	8.7
10 MeV protons	4.9	187	9.3	8.8	8.8
5 MeV protons	8.5	183	9.9	9.4	9.3
4 MeV protons	10.6	179	10.1	9.5	9.4
3 MeV protons	13.3	180	10.5	9.8	9.5
2 MeV protons	18.5	171	11.6	10.7	10.2
1.5 MeV protons	23.3	166	12.6	11.4	10.5
1 MeV protons	32.5	153	14.4	12.3	11.2
0.8 MeV protons	40.6	146	15.8	12.7	11.6
0.7 MeV protons	47.1	138	16.3	12.6	11.2
0.6 MeV protons	56.1	123	17.0	12.1	10.6
0.5 MeV protons	69.7	110	18.7	12.1	10.1
⁶⁰ Co γ rays	0.4	195	8.7	8.3	8.3
220 kVp X rays	4.3	188	9.7	9.1	9.1
10 MeV electrons	0.23	197	8.2	7.9	7.9

^a Data for protons and electrons were determined from simulated tracks, data for photons from Blohm (see footnote 3).

^b Data disregarding multiple DSBs within 10 kbp.

^c Data determined from linear regression of dose-dependent yields according to Eq. (1) for an exclusion fragment size of 1 Mbp.

$$F_{bg} = k_{\min} \left[1 - R \left(1 - \frac{k_{\max}}{k_{\min}} \right)^{B+1} \right]^{1/(B+1)} \quad (4)$$

From the recently measured distribution of background fragments (9), parameter values of $A = 2 \times 10^{-6} \text{ bp}^{-2}$ and $B = -1.4$ were derived. Background DNA fragments were sampled by Monte Carlo methods according to Eq. (4) within the fragment size interval between 10 kbp and 10 Mbp. DNA DSBs generating these fragments were assumed to be located at the telomeres of all chromosomes in each cell to rule out an alteration of the distribution due to the unbroken remainder of chromosomes. After superimposition of the background DSBs with the radiation-induced DSBs, size distributions of DNA fragments were analyzed to study inaccuracies induced by calculating radiation-induced fragment distributions by simple subtraction of background distributions from those measured after irradiation. It must be noted that this model is designed

to show possible implications of background distributions without respect to the real origin of these background fragments.

Irradiation Geometry and Simulation Calculations

In a typical experimental setup, a single layer of cells grown on a thin foil is irradiated by a parallel beam of primary radiation protons, electrons or photons passing perpendicular through the foil. In the present simulation a single human fibroblast from this layer was modeled by a cylinder with a diameter of 20 μm and a height of 6 μm placed with a flat side on a 1.5-μm-thick Mylar foil. The cell consisted of a concentric cylindrical cell nucleus 15 μm in diameter and 5 μm high with the DNA target embedded as described above, surrounded by cell plasma. For both cell constituents a mass density of 1.06 g/cm³ was applied by which the liquid water cross sections were scaled.

Simulation calculations were performed for protons with initial energies between 0.5 and 50 MeV, and three reference radiation qualities: electrons of 10 MeV initial energy, ⁶⁰Co γ rays and 220 kVp X rays with a spectrum produced by filtering with 0.5 mm copper + 4 mm aluminum. Proton energies and LET values are presented in Table 1. Protons of 0.5 MeV are stopped in the cell plasma shortly after penetrating the nucleus. They provide the maximum achievable LET of about 70 keV/μm for this particle type. One hundred irradiation simulations of a dose of 1 Gy, corresponding to a total energy deposition of 5.85 MeV within the cell nucleus, were performed for each radiation type and each initial proton energy. The results were compared with experimental data on the basis of the reported LET.

RESULTS AND DISCUSSION

Induction of DNA Strand Breaks

In Fig. 2, the yield for the induction of DNA strand breaks (including the breaks scored as DSBs) is plotted as a function of the LET of the radiation type. The contributions from direct and from indirect effects are also given. Numerical results are included in Table 1. For 10 MeV electrons, γ rays and X rays, similar yields are obtained as

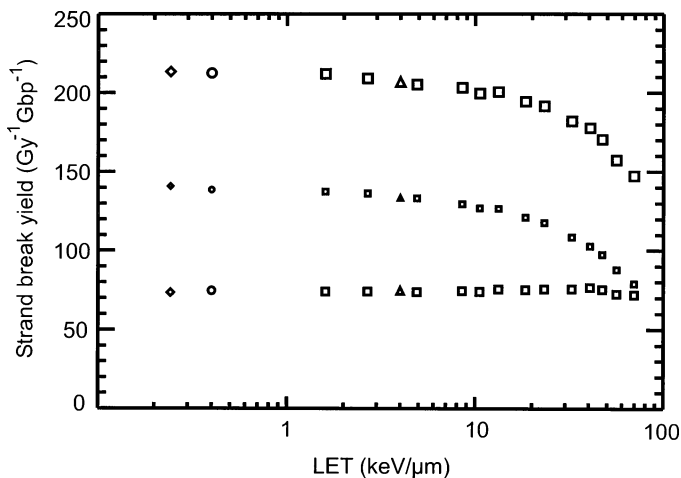


FIG. 2. Calculated yield of DNA strand breaks (large symbols) and contributions of direct (medium-sized symbols) and indirect effects (small symbols) after irradiation with protons (□), ⁶⁰Co γ rays (○), 220 kVp X rays (△), and 10 MeV electrons (◇). Pairs of breaks scored as DSBs are included as two breaks.

for high-energy protons. For proton irradiation with an LET above 10 keV/ μm , the total yield of breaks decreases with increasing LET by up to 30%. This reduction is caused by a more pronounced decrease in the indirect contribution, whereas the yields from direct effects are almost independent of LET and radiation type. Thus the relative contribution of direct effects to the total yield increases with LET from about 35% for low-LET radiation up to nearly 50% for high-LET radiation. For DNA strand break induction, the same tendency was found by Nikjoo *et al.* (36); however, they obtained a smaller decrease of about 12% within the LET range from 9 to 59 keV/ μm , whereas a decreasing contribution of indirect effects with increasing LET was found only in comparison to electron irradiation and for α particles.

The independence of strand break induction due to direct effects from radiation quality reflects a rather limited influence of the geometric track structures on the breakage mechanism. Earlier calculations resulted in a reduced induction of breaks for electron energies around 300 eV where the maximum density of events occurred. Thus a decrease for high-LET protons has been expected. In the present work, however, the breakage probability increases with deposited energy. Therefore, a second and even a third hit at the same base pair—which are much more frequent for high-LET protons than for ^{60}Co γ rays—has an effectiveness for strand break induction similar to that of the first hit. With the strand breakage parameter set used in earlier simulations, a decline is obtained in the strand break yield from direct effects approaching up to 20% for protons of 70 keV/ μm .

The decrease in the strand break yield due to indirect effects with increasing LET for proton irradiations is a consequence of the structure of the proton track. The yield of OH radicals at the beginning of the chemical stage is quite similar for the different radiation qualities considered; this is also the case for interactions of OH radicals with DNA during the first picoseconds. However, due to the shorter mean free path after high-LET irradiation, the radicals find more reaction partners during the time course of the chemical stage. Therefore, a smaller number of radicals remain for diffusing to and reacting with the DNA constituents.

Yields of DNA Double-Strand Breaks and Short DNA Fragments

In Fig. 3, simulated yields for the induction of DSBs are presented as a function of the LET on a linear scale; the numerical data are included in Table 1. The DSB yield after proton irradiation increases about linearly with LET; above about 25 keV/ μm , the slope of this increase is slightly reduced. The yields for electron and photon irradiation fit well on the regression line of a second-order polynomial fit of proton data. These results are in good agreement with the simulations of Nikjoo *et al.* (36). A linear increase with increasing LET has been found before for photons and α

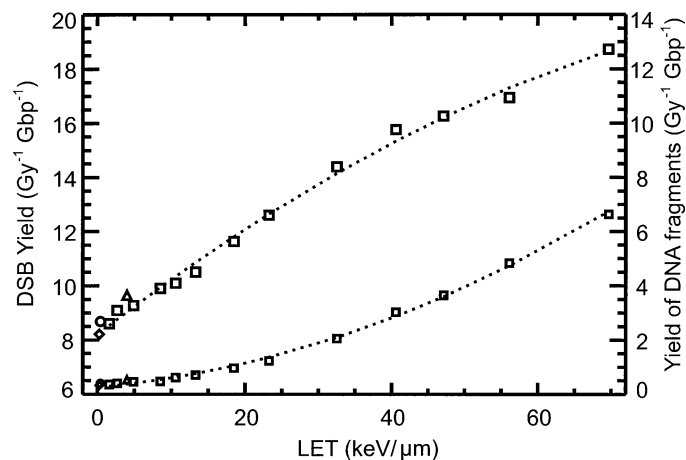


FIG. 3. Calculated yield of DNA DSBs (large symbols, left scale) and of DNA fragments < 10 kbp (small symbols, right scale) after irradiation with protons (\square), ^{60}Co γ rays (\circ), 220 kVp X rays (\triangle), and 10 MeV electrons (\diamond).

particles, yielding about the same slope ($0.2 \text{ DSB Gy}^{-1} \text{ Gbp}^{-1}$ per keV/ μm) on the basis of restricted LET.² Considering the reduced induction of strand breaks with LET, it turns out that this is overcompensated by an increased probability of having a second break on the opposite strand in the vicinity of a first one, whereas the contribution of DSBs from single interactions reduces the LET dependence.

In Fig. 3, the generation of double-stranded fragments of up to 10 kbp fragment size is also plotted using the same differential scale but a shift in the absolute values (right-hand scale). The production of these DNA fragments shows an almost quadratic increase with increasing LET with a small offset. Again, the results for photons and electrons fit well into the general trend of the proton data. The dependence on radiation quality is much more pronounced for this fragment production than for DSB induction. It is also more distinct than the induction of complex breaks (36), which increases by a factor of about 4 within the LET range investigated (9–59 keV/ μm). It depends particularly on the compactness of the chromatin fiber: Compared to the results of the calculations in the pilot study (15) using a slightly less compact fiber, the fragment production is enhanced by about 20%, whereas the same DSB yield has been obtained.

In Fig. 4, the simulated DSB yields, presented as a function of LET on a logarithmic scale, are compared with experimental results that also illustrate the contribution of experimentally unresolved small fragments. In Fig. 5, the same results are plotted as relative DSB yields compared

² E. Bartels, Der beschränkte lineare Energietransfer als statistische Kenngröße der Teilchenbahnstruktur in der Strahlenphysik. Thesis, Georg-August-Universität Göttingen, 1995. [in German]

³ R. Blohm, Durchgang von Elektronen durch strahlenempfindliche Bereiche des Zellkerns. Thesis, Georg-August-Universität Göttingen, 1983. [in German]

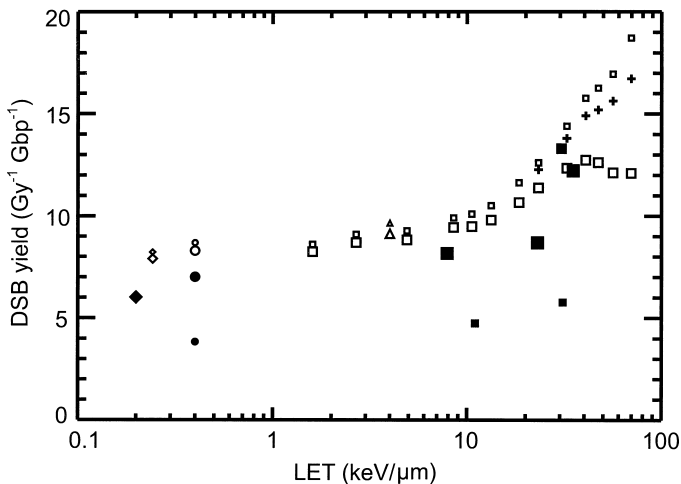


FIG. 4. Calculated yield of total (small open symbols) and “distant” DNA DSBs after exclusion of multiple breaks within 10 kbp (large open symbols) after irradiation with protons (□), ^{60}Co γ rays (○), 220 kVp X rays (△), and 10 MeV electrons (◇), compared to experimental results for protons (■) from refs. (7) (large symbols), (8) (small symbols) and (9) (medium-sized symbol) and for reference radiation [15 MeV electrons (◇) from ref. (7), ^{60}Co γ rays (●) from (8) (small symbol) and (9) (medium-sized symbol)]. Calculated results after exclusion of multiple breaks within 200 bp are indicated by (+).

to ^{60}Co γ rays as the reference radiation. Recent experimental results (7–9) are included in both plots. The RBE data reported by Frankenberg *et al.* (7) are adjusted for the reduced yield of the 15 MeV electron reference radiation according to the relation of DSB yields for 10 MeV electrons to ^{60}Co γ rays in the simulations.

The exclusion of small fragments has little influence in the DSB yield up to an LET of about 10 keV/ μm and, since a similar impact occurs for the reference radiation, almost no effect on the RBE. With increasing LET, however, the increase in the number of small fragments becomes steeper and eventually exceeds the increase in the number of DSBs, which leads to a maximum in the yield of distant DSBs and the corresponding RBE at about 40 keV/ μm . Limiting the exclusion of fragments to 200 bp does not alter the general shape of the curve for total DSB induction but reduces its steepness.

With one exception, the simulated DSB yields are higher than recent experimental data and far above earlier measurements [(2), not included in the figure]. The RBE for DSB induction after proton irradiation, however, is smaller than these recent experimental results in all but one case. Earlier experimental RBE values of the order of 1 and below [(2), not shown] are not in accordance with the simulated results.

The simulation results depend on the DNA target model and on the parameters for strand breakage. The high compactness of the chromatin fiber used gives rise to high numbers of small fragments but slightly lower numbers of total breaks. With a somewhat less compact fiber, no decrease but an almost constant yield of distant DSBs was obtained

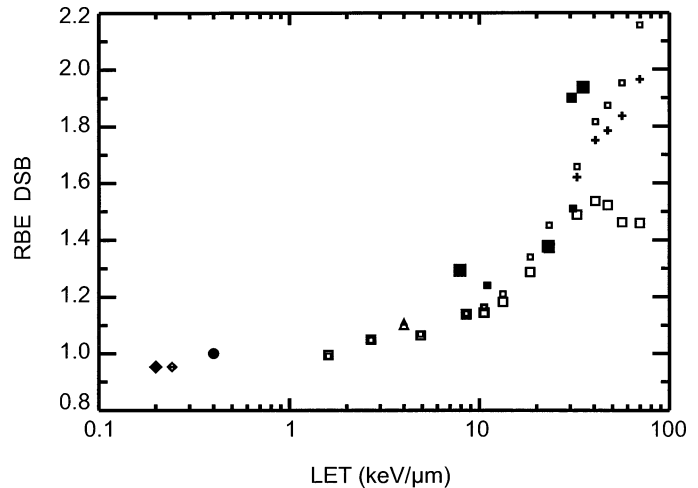


FIG. 5. Calculated RBE of total (small open symbols) and “distant” DNA DSBs after exclusion of multiple breaks within 10 kbp (large open symbols) after irradiation with protons (□), ^{60}Co γ rays (○), 220 kVp X rays (△), and 10 MeV electrons (◇), compared to experimental results for protons (■) from refs. (7) (large symbols), (8) (small symbol) and (9) (medium-sized symbol). Calculated results after exclusion of multiple breaks within 200 bp are indicated by (+). RBE values are relative to ^{60}Co γ rays (●); data from ref. (7) are scaled by matching the result for 15 MeV electrons (◇) with the simulated RBE for 10 MeV electrons.

at the highest LET values considered (15). In our simulation the genome is totally packed in 30-nm chromatin fiber rods, whereas in real interphase cells active chromatin regions are thought to be less densely folded. In such regions enhanced DSB induction can be expected due to greater accessibility to OH radicals. For a “beads-on-a-string” form, an increase by a factor of about 2 has been obtained for γ rays (publication in preparation), whereas the production of short fragments is reduced due to the lack of pieces of DNA in proximity. These factors may reduce the deviations between simulation and measurement; however, a detailed analysis of such effects of chromatin packing is outside the scope of this work. Nevertheless, it can be concluded that the compactness of the chromatin fiber and the fraction of DNA being folded into such a structure are important determinants of the DSB yield, particularly after proton irradiation with an LET of more than about 20 keV/ μm .

The simulated DSB yields in Fig. 4 correspond to data obtained by counting the number of fragments. These data may also be derived directly from measurements of DNA fractions in many narrow fragment intervals (11). The experimental data included in that figure, however, were calculated from the fractions of activity released from the well under CFGE or PFGE after irradiation. In Fig. 6, calculated DSB yields derived from simulated fractions of DNA by applying Eq. (1) are presented as a function of the (gel) exclusion fragment size for different radiation doses and from a linear regression of these dose-dependent DSB yields. The data are compared with simulated yields of distant DSBs because the contribution of DSBs associated

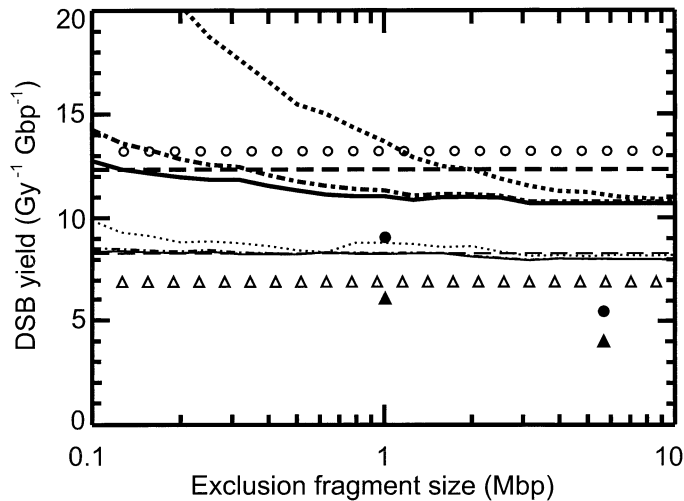


FIG. 6. Calculated yield of DNA DSBs for 1 MeV protons (thick lines) and ^{60}Co γ rays (thin lines) from FAR analysis (Eq. 1) of DNA fragments after irradiation with 10 Gy (dotted line), and 100 Gy (dashed-dotted line) and from linear regression (solid line). The horizontal dashed lines indicate the calculated yields of distant DSBs (multiple breaks within 10 kbp excluded). Experimental yields (12) for 31 keV/ μm protons (\bullet , \circ) and ^{60}Co γ rays (\blacktriangle , \triangle) obtained by FAR method (filled symbols) and by fragment counting method (open symbols) are included.

with small DNA fragments to the total yield cannot be estimated from data on larger fragments. Moreover, very recent experimental data obtained with the FAR method for two exclusion fragment sizes and with fragment counting are included (12).

The DSB yields derived for 1 MeV protons depend strongly on the exclusion size adopted; particularly for low doses and small exclusion fragment sizes, increased DSB yields are obtained. For exclusion fragment sizes above 1 Mbp, however, the results after 100 Gy with linear regression are almost constant, with a value below the actual yield of distant DSBs. Thus the FAR method may result in an underestimation of the DSB yield. For ^{60}Co γ rays, only a marginal dependence of the simulated DSB yields on the analysis method is found; for exclusion fragment sizes above 2 Mbp, the DSB yield from the FAR method is about 5% below the corresponding yield of distant DSBs. These tendencies in the simulated DSB yields from FAR analysis are confirmed by the new experimental data (12); however, the differences in the results are much more pronounced in the experimental results and thus are challenging us to refine the simulation calculations.

Distribution of DNA Fragments

The radiation-induced production of DNA DSBs along the genome generates double-stranded DNA fragments with a size distribution that depends on dose and radiation quality. In Fig. 7, the thick lines represent simulated DNA fragment size distributions as fractions of DNA found in double-stranded fragments per size interval, after 100 Gy irradiation with 0.5 MeV protons, 3 MeV protons, and ^{60}Co

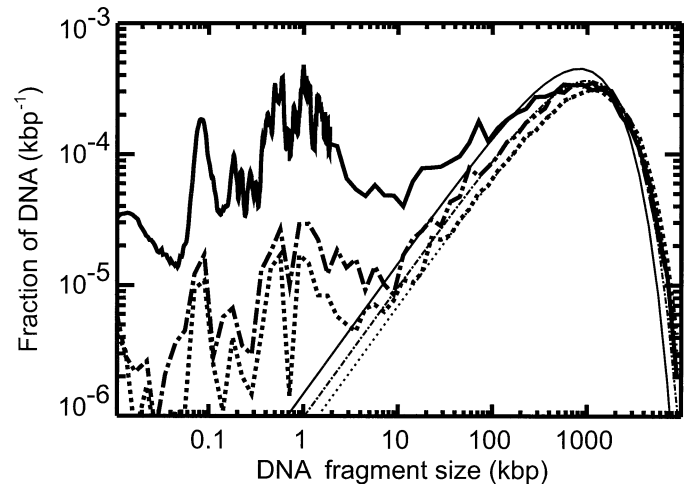


FIG. 7. Calculated DNA fragment distribution after 100 Gy irradiation with protons of 0.5 MeV (solid line) and 3 MeV (dashed-dotted line) and ^{60}Co γ rays (dotted line). Thin lines indicate random breakage distributions for the corresponding numbers of distant DSBs (multiple breaks within 10 kbp excluded).

γ rays. The thin lines in the figure represent the corresponding distributions assuming randomly induced DSBs for the same numbers of distant DSBs. The total spectrum of DNA fragment sizes can be divided into two domains: small DNA fragments up to a few kbp and large DNA fragments with sizes above that value. The small fragments, which are presented for 0.5 MeV protons in a better resolution are produced predominantly by single tracks, and the number of fragments increases linearly with dose. The peak structure reflects the organization of the nucleosomes within the chromatin fiber independent from radiation quality and dose within the radiation types and range of doses considered here. Groups of peaks around 0.5, 1 and 1.5 kbp are perceptible but less pronounced than for earlier simulated regular crossed-linker arrangements (16, 17), although they are more distinct than the corresponding experimental distributions (37).

In the distributions of larger DNA fragments the single-track component is overlaid—with increasing dose and fragment size more and more—by a random breakage distribution originating from fragments between DSBs from two independent tracks. After 0.5 MeV proton irradiation, the distribution obviously deviates from a random breakage curve even at this dose of 100 Gy. Two intersection points of both distributions divide the distribution into three domains. Whereas small fragments up to about 100 kbp and large fragments of more than 2.5 Mbp are more frequent, the fragments in the interval around the maximum in the simulated distribution are reduced by up to 25% compared to the random distribution. This reduced maximum, which is not compensated by the higher number of small fragments, is the explanation for the reduced DSB yield from FAR analysis. No such difference is seen around the peak region for the other radiation qualities presented. Indications for a deviation from random breakage are visible for

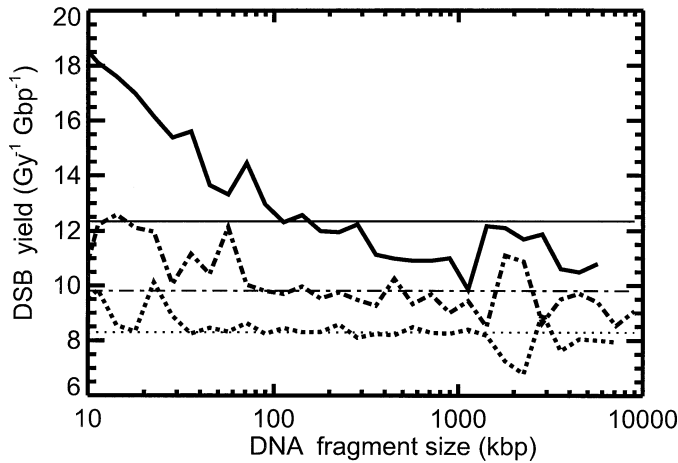


FIG. 8. Calculated fragment size-dependent DNA DSB yields after 100 Gy irradiation with protons of 1 MeV (solid line) and 3 MeV (dashed-dotted line) initial energy and ^{60}Co γ rays (dotted line). The horizontal thin lines indicate the corresponding yields of distant DSBs (multiple breaks within 10 kbp excluded).

fragments up to about 50 kbp after 3 MeV proton irradiation, whereas for ^{60}Co γ rays significant differences are limited to small fragments below 10 kbp.

A more sensitive analysis of deviations of simulated DNA fragment patterns from random breakage distributions results from conversion of the DNA fragment yields to fragment size-dependent DSB yields according to Eq. (2). Corresponding DSB yields are presented in Fig. 8 on a linear scale for irradiation with 100 Gy. For ^{60}Co γ rays, the DSB yield is constant above about 50 kbp and is close to the distant DSB yield. The same result is found for protons of 10 MeV or more initial energy and for the other reference radiation qualities (not shown). For 3 MeV protons, a tendency toward higher DSB yields for smaller fragment sizes is perceptible, whereas for 1 MeV protons the yield decreases by a factor of about 1.8 between 10 and 1000 kbp. The peak at about 70 kbp is a consequence of the position of the two pieces of DNA being four chromatin fiber rods apart from each other, whereas the rise at 1.5 Mbp originates from switching the branch of the fragment distribution (see the Materials and Methods). To summarize, DNA fragments from single tracks contribute observably to the simulated DNA fragment distribution even after 100 Gy of irradiation with protons having an LET of more than 10 keV/ μm .

In Fig. 9, simulated distributions of background and total DNA fragments after 100 Gy irradiation with 1 MeV protons or ^{60}Co γ rays are presented and compared with the corresponding experimental results (9). The initial proton energy in the experiment was 3 MeV, but the reported LET of 31 keV/ μm and proton energy of 0.743 MeV in the cell midplane at a depth of 3 μm are similar to the corresponding simulated data for 1 MeV protons (32.5 keV/ μm and 0.845 MeV, respectively). The simulated background distribution has been fitted to the measured data and is found

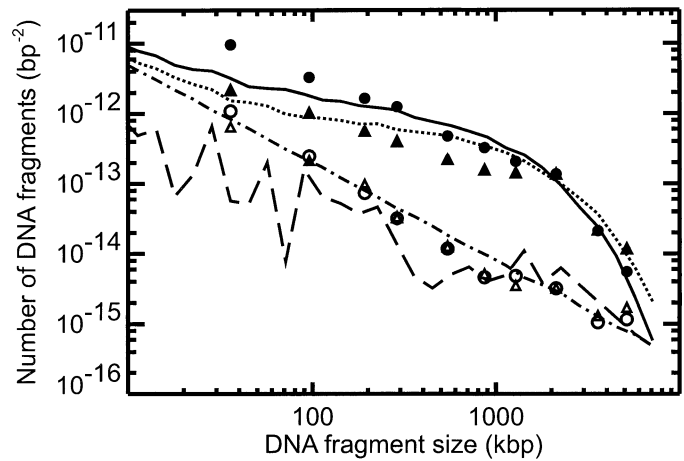


FIG. 9. Calculated DNA fragment distribution after 100 Gy irradiation with 1 MeV protons (solid line) and ^{60}Co γ rays (dotted line) considering background fragments (dashed-dotted line), compared with experimental results (9) after 100 Gy irradiation with protons (\square) and ^{60}Co γ rays (π) and corresponding background fragment distributions (\square, ρ). The dashed line indicates the absolute difference between simulations for 1 MeV protons with and without consideration of background fragments.

to be in agreement. For both radiation qualities, the experimental and simulated results are in good agreement for DNA fragments larger than 2 Mbp, and the intersection of both distributions at this fragment size is reproduced. However, for small fragments (below 100 kbp), particularly after proton irradiation, the simulation underestimates the measured data, whereas for fragments between 0.4 and 1.3 Mbp the simulation exceeds the experimental results, especially for γ rays. The inclusion of higher-order DNA structures altered the distribution from random breakage behavior in the right direction but not sufficiently. The remaining difference corresponds to factors of 2 and 3 at 100 and 35 kbp, respectively. This may be an indication of a more closed and more compact fiber loop structures, e.g. attachment points at the loop ends and twisted chromatin fibers, than in the layout assumed in the simulation.

The difference between simulations for 1 MeV protons with and without consideration of the background distribution is presented by the dashed line; the background contributes a fraction of less than one-tenth of the distribution. Simple subtraction of the background distribution from the measured distribution produces an error that can be neglected in view of the uncertainties of such measured data. This implies, however, that the unknown mechanism responsible for the generation of a background distribution in unirradiated cells does not increase the yield of DNA DSBs in response to the radiation-induced DNA damage.

CONCLUSION

The present simulations have demonstrated the importance of DNA DSBs from single tracks after irradiation with protons with an LET greater than about 10 keV/ μm . Multiple DSBs were found to occur predominantly within

the chromatin fiber structure and to a minor degree within the nucleosome. A comparison of the experimental and simulated induction of DNA DSBs after proton irradiation of cells, and even more after α -particle or heavy-ion irradiation, should take into account clusters of DSBs within the chromatin fiber that remain unresolved in experiments. Simple DNA target models describing just a double helix are not sufficient for an adequate evaluation, and even a nucleosome model may account for less than half of the contribution of multiple breaks. This result is derived under the assumption that cellular DNA is packed in highly condensed chromatin fibers; because of the presence of different degrees of DNA folding within the chromosomes, the amount of DSB clusters within the chromatin fiber may be overestimated in the simulation. Indeed, the variation of calculated RBE of "distant" DSBs due to radiation quality is notably smaller than the variation in the corresponding experimental results, whereas this comparison based on the RBE for total DSBs shows reasonable agreement.

The analysis of DNA DSB yields using algorithms derived under the assumption of random breakage may cause deviations from the actual yields. Conditions leading to overestimation of the DSB yield (low radiation doses and rather small DNA exclusion fragment sizes) should be irrelevant in analysis of experimental data. However, the reduced maximum in the distribution of DNA fractions as a function of fragment size may cause a considerable underestimation of the DSB yields, and a recent study (12) underlines this problem of using relationships derived under random breakage conditions in the FAR method for DSB determination. After α -particle or heavy-ion irradiation, which have higher LET, even more substantial underestimations must be expected. In combination with the unresolved DSBs associated with small fragments this should explain the surprisingly low experimental RBE values for DSB induction, particularly after high-LET irradiation.

In our simulation the consideration of background DNA fragments does not alter the net yield of radiation-induced fragments significantly, provided that the DNA breaks causing the background distribution are formed similarly in irradiated and nonirradiated cells. The limited degree of conformity between simulated and experimental distributions of DNA fragments continues to challenge models for DNA damage simulation.

ACKNOWLEDGMENTS

This work was supported by European Union (contract number FIGH-CT1999-00005). MD expresses appreciation for a Marie Curie Fellowship from the European Union (contract number FIGH-CT-1999-50002).

Received: April 26, 2002; accepted: October 14, 2002

REFERENCES

1. C. von Sonntag, *The Chemical Basis of Radiation Biology*. Taylor & Francis, London and New York, 1987.
2. K. M. Prise, G. Ahnstrom, M. Belli, J. Carlsson, D. Frankenberg, J. Kiefer, M. Lobrich, B. D. Michael, J. Nygren and B. Stenerlow, A review of dsb induction data for varying quality radiations. *Int. J. Radiat. Biol.* **74**, 173–184 (1998).
3. K. M. Prise, M. Pinto, H. C. Newman and B. D. Michael, A review of studies of ionizing radiation-induced double-strand break clustering. *Radiat. Res.* **156**, 572–576 (2001).
4. M. Belli, F. Cera, R. Cherubini, F. Ianzini, G. Moschini, O. Sapora, G. Simone, M. A. Tabocchini and P. Tiveron, DNA double-strand breaks induced by low energy protons in V79 cells. *Int. J. Radiat. Biol.* **65**, 529–536 (1994).
5. T. J. Jenner, M. Belli, D. T. Goodhead, F. Ianzini, G. Simone and M. A. Tabocchini, Direct comparison of biological effectiveness of protons and alpha-particles of the same LET. III. Initial yield of DNA double-strand breaks in V79 cells. *Int. J. Radiat. Biol.* **61**, 631–637 (1992).
6. K. M. Prise, M. Folkard, S. Davies and B. D. Michael, The irradiation of V79 mammalian cells by protons with energies below 2 MeV. Part II. Measurement of oxygen enhancement ratios and DNA damage. *Int. J. Radiat. Biol.* **58**, 261–277 (1990).
7. D. Frankenberg, H. J. Brede, U. J. Schrewe, C. Steinmetz, M. Frankenberg-Schwager, G. Kasten and E. Pralle, Induction of DNA double-strand breaks by ^1H and ^4He ions in primary human skin fibroblasts in the LET range of 8 to 124 keV/nucleon. *Radiat. Res.* **151**, 540–549 (1999).
8. M. Belli, R. Cherubini, M. Dalla Vecchia, V. Dini, G. Moschini, C. Signoretti, G. Simone, M. A. Tabocchini and P. Tiveron, DNA DSB induction and rejoining in V79 cells irradiated with light ions: A constant field gel electrophoresis study. *Int. J. Radiat. Biol.* **76**, 1095–1104 (2000).
9. M. Belli, R. Cherubini, M. Dalla Vecchia, V. Dini, G. Esposito, G. Moschini, O. Sapora, C. Signoretti, G. Simone and M. A. Tabocchini, DNA fragmentation in mammalian cells exposed to various light ions. *Adv. Space Res.* **27**, 393–399 (2001).
10. B. Cedervall, R. Wong, N. Albright, J. Dynlacht, P. Lambin and W. C. Dewey, Methods for the quantification of DNA double-strand breaks determined from the distribution of DNA fragment sizes measured by pulsed-field gel electrophoresis. *Radiat. Res.* **143**, 8–16 (1995); Erratum, *Radiat. Res.* **144**, 122 (1995).
11. M. Pinto, K. M. Prise and B. D. Michael, Quantification of radiation induced DNA DSBs in human fibroblasts by PFGE: Testing the applicability of random breakage models. *Int. J. Radiat. Biol.* **78**, 375–388 (2002).
12. M. Belli, R. Cherubini, M. Dalla Vecchia, V. Dini, G. Esposito, G. Moschini, O. Sapora, G. Simone and M. A. Tabocchini, DNA fragmentation in V79 cells irradiated with light ions as measured by pulsed-field gel electrophoresis. I. Experimental results. *Int. J. Radiat. Biol.* **78**, 475–482 (2002).
13. M. Pinto, H. C. Newman, K. M. Prise and B. D. Michael, Quantification of DNA damage by PFGE: Development of an analytical approach to correct for the background distribution. *Int. J. Radiat. Biol.* **76**, 741–748 (2000).
14. H. C. Newman, K. M. Prise and B. D. Michael, The role of higher-order chromatin structure in the yield and distribution of DNA double-strand breaks in cells irradiated with X-rays or alpha-particles. *Int. J. Radiat. Biol.* **76**, 1085–1093 (2000).
15. W. Friedland, P. Bernhardt, P. Jacob, H. G. Paretzke and M. Dingfelder, Simulation of DNA damage after proton and low-LET irradiation. *Radiat. Prot. Dosim.* **99**, 99–102 (2002).
16. W. Friedland, P. Jacob, H. G. Paretzke and T. Stork, Monte Carlo simulation of the production of short DNA fragments by low-linear energy transfer radiation using higher-order DNA models. *Radiat. Res.* **150**, 170–182 (1998).
17. W. Friedland, P. Jacob, H. G. Paretzke, M. Merzagora and A. Ottolenghi, Simulation of DNA fragment distributions after irradiation with photons. *Radiat. Environ. Biophys.* **38**, 39–47 (1999).
18. M. Dingfelder, M. Inokuti and H. G. Paretzke, Inelastic-collision cross sections of liquid water for interactions of energetic protons. *Radiat. Phys. Chem.* **59**, 255–275 (2000).

19. M. Dingfelder, D. Hantke, M. Inokuti and H. G. Paretzke, Electron inelastic-scattering cross sections in liquid water. *Radiat. Phys. Chem.* **53**, 1–18 (1998).
20. ICRU, *Stopping Powers and Ranges for Protons and Alpha Particles*. Report 49, International Commission on Radiation Units and Measurements, Bethesda, MD, 1993.
21. M. Dingfelder, Cross section calculations in condensed media—charged particles in liquid water. *Radiat. Prot. Dosim.* **99**, 23–28 (2002).
22. C. M. de Lara, M. A. Hill, T. J. Jenner, D. Papworth and P. O'Neill, Dependence of the yield of DNA double-strand breaks in Chinese hamster V79–4 cells on the photon energy of ultrasoft X rays. *Radiat. Res.* **155**, 440–448 (2001).
23. J. Nygren, M. Ljungman and G. Ahnstrom, Chromatin structure and radiation-induced DNA strand breaks in human cells: Soluble scavengers and DNA-bound proteins offer a better protection against single- than double-strand breaks. *Int. J. Radiat. Biol.* **68**, 11–18 (1995).
24. B. D. Michael and P. O'Neill, A sting in the tail of electron tracks. *Science* **287**, 1603–1604 (2000).
25. B. Boudaiffa, P. Cloutier, D. Hunting, M. A. Huels and L. Sanche, Resonant formation of DNA strand breaks by low-energy (3 to 20 eV) electrons. *Science* **287**, 1658–1660 (2000).
26. K. M. Prise, M. Folkard, B. D. Michael, B. Vojnovic, B. Brocklehurst, A. Hopkirk and I. H. Munro, Critical energies for SSB and DSB induction in plasmid DNA by low-energy photons: Action spectra for strand-break induction in plasmid DNA irradiated in vacuum. *Int. J. Radiat. Biol.* **76**, 881–890 (2000).
27. V. V. Moiseenko, R. N. Hamm, A. J. Waker and W. V. Prestwich, Calculation of radiation-induced DNA damage from photons and tritium beta-particles. Part I: Model formulation and basic results. *Radiat. Environ. Biophys.* **40**, 23–31 (2001).
28. F. Ballarini, M. Biaggi, M. Merzagora, A. Ottolenghi, M. Dingfelder, W. Friedland, P. Jacob and H. G. Paretzke, Stochastic aspects and uncertainties in the prechemical and chemical stages of electron tracks in liquid water: A quantitative analysis based on Monte Carlo simulations. *Radiat. Environ. Biophys.* **39**, 179–188 (2000).
29. G. V. Buxton, C. L. Greenstock, W. P. Helman and A. B. Ross, Critical review of rate constants for reactions of hydrated electrons, hydrogen atoms and hydroxyl radicals in aqueous solution. *J. Phys. Chem. Ref. Data* **17**, 513–886 (1988).
30. R. N. Hamm, J. E. Turner and M. G. Stabin, Monte Carlo simulation of diffusion and reaction in water radiolysis—a study of reactant 'jump through' and jump distances. *Radiat. Environ. Biophys.* **36**, 229–234 (1998).
31. J. R. Milligan, J. A. Aguilera and J. F. Ward, Variation of single-strand break yield with scavenger concentration for plasmid DNA irradiated in aqueous solution. *Radiat. Res.* **133**, 151–157 (1993).
32. V. V. Moiseenko, R. N. Hamm, A. J. Waker and W. V. Prestwich, The cellular environment in computer simulations of radiation-induced damage to DNA. *Radiat. Environ. Biophys.* **37**, 167–172 (1998).
33. M. A. Siddiqi and E. Bothe, Single- and double-strand break formation in DNA irradiated in aqueous solution: Dependence on dose and OH radical scavenger concentration. *Radiat. Res.* **112**, 449–463 (1987).
34. B. Cedervall and P. Kallman, Randomly distributed DNA double-strand breaks as measured by pulsed field gel electrophoresis: A series of explanatory calculations. *Radiat. Environ. Biophys.* **33**, 9–21 (1994).
35. C. R. Contopoulou, V. E. Cook and R. K. Mortimer, Analysis of DNA double strand breakage and repair using orthogonal field alternation gel electrophoresis. *Yeast* **3**, 71–76 (1987).
36. H. Nikjoo, P. O'Neill, W. E. Wilson and D. T. Goodhead, Computational approach for determining the spectrum of DNA damage induced by ionizing radiation. *Radiat. Res.* **156**, 577–583 (2001).
37. B. Rydberg, W. R. Holley, I. S. Mian and A. Chatterjee, Chromatin conformation in living cells: support for a zig-zag model of the 30 nm chromatin fiber. *J. Mol. Biol.* **284**, 71–84 (1998).